Controllability and Resiliency Analysis for a Heat-Integrated C_3-Splitter*

Boris M. Solovyev and Daniel R. Lewin†
Wolfson Department of Chemical Engineering
Technion –IIT
Haifa 32000, Israel

Abstract

Controllability and resiliency (C&R) diagnosis is carried out on an industrial heat-integrated propane/propylene distillation column (C_3-splitter). The analysis is based on short-cut dynamic models, which are obtained directly from the steady-state material and energy balances solved using a commercial process simulator. The results indicate that the designed operating point is open loop unstable. Systematic C&R screening of all of the alternative decentralized control configurations suggests that the preferable control pairings are in line with current efforts to stabilize the process. However, the severe bandwidth limitations due to dynamic interactions for the best possible decentralized configuration imply that multivariable control is required for adequate performance.

Keywords: Controllability and resiliency assessment, Process design, Heat-integrated processes, Distillation.

1 Introduction

The inclusion of controllability and resiliency (C&R) analysis in the early stages of process design in an important part of any modern design approach (Seider *et al*., 1999). One of the main reasons that C&R analysis is not commonly carried out is the absence of a reliable dynamic model, which in most cases is not prepared in the early design stages. However, using the approach described by Weitz and Lewin (1996), it is possible to generate an approximate linear dynamic model for process flowsheets in the vicinity of the desired operating point. This approach relies on the partition of the flowsheet into so-called "component parts", each of which is expressed in terms of a matrix of low-order transfer functions. Since the way that the flowsheet is partitioned into its component-parts has bearing on the overall dynamics of the process model, this step should therefore be carried out carefully. The static gains of the component-part transfer matrices are derived either by perturbation analysis, or by

* The authors gratefully acknowledge the supported of this research by Carmel Olefins Ltd., Haifa

† Author to whom all correspondence should be addressed. Email: *dlewin@tx.technion.ac.il*.

analytical differentiation of an interpolation polynomial fitted to the simulated variation of the output variables to each of its inputs. The time constants are computed based on vessel capacities, which are available after equipment sizing is completed, and the designed vessel throughputs. The overall process model is obtained by algebraic manipulations of the component-part transfer matrices (Lewin *et al*., 1996). The general form of the process dynamic model is:

$$\underline{\boldsymbol{y}}(s) = \underline{\underline{\boldsymbol{P}}}(s)\,\underline{\boldsymbol{u}}(s) + \underline{\underline{\boldsymbol{P}}}_d(s)\,\underline{\boldsymbol{d}}(s) \tag{1}$$

where s is the Laplace variable, $\underline{\boldsymbol{y}}(s)$ is a vector of process outputs, $\underline{\boldsymbol{u}}(s)$ is a vector of process inputs, $\underline{\boldsymbol{d}}(s)$ is a vector of process disturbances, and $\underline{\underline{\boldsymbol{P}}}(s)$ and $\underline{\underline{\boldsymbol{P}}}_d(s)$ are process transfer matrices that connect outputs with inputs and disturbances respectively. The linear approximation in Eq.(1) is then used to test the controllability and resiliency of the process flowsheet using the linear measures available in the literature; Lewin (1999) gives a review of the commonly used linear controllability measures.

This approach has been used successfully for screening complex heat-integrated flowsheets (Weitz, 1994; Solovyev *et al*., 1998), exothermic reactors (Naot and Lewin, 1995, Seider *et al*., 1999), polymerization reactors (Lewin and Bogle, 1996), and processes featuring material recycle (Naot and Lewin, 1995; Lewin *et al*., 1996). In all of these studies, the short-cut C&R analysis reproduces the conclusions obtained by others, largely using rigorous dynamic models. Furthermore, as in the case study described in this paper, all of these reported studies make use of the *relative-gain array* (RGA, Bristol, 1966) and the *disturbance cost* (DC, Lewin, 1996) to test controllability and resiliency measures respectively. The main advantage of using these measures is that the C&R analysis assumes perfect control arguments, and is thus independent of controller tuning, but sensitive to the process design and control configuration (e.g., decentralized control).

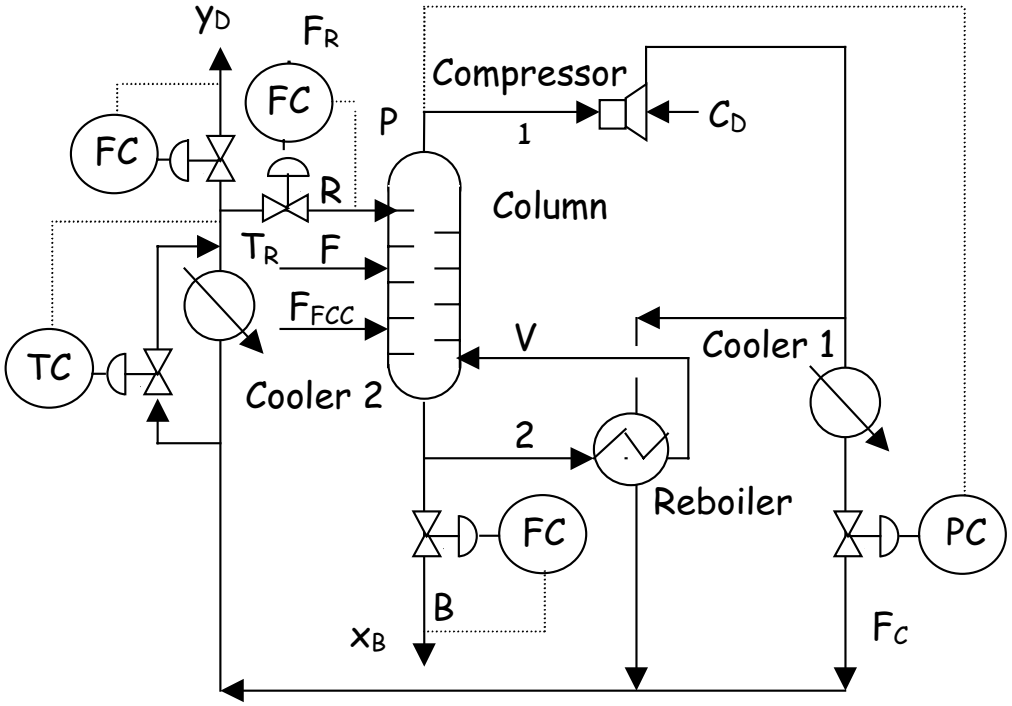

Figure 1. Original process configuration.

2 Process Description and Control Objectives

A heat-integrated propylene/propane (C_3-) splitter purifies the propylene fed to a down stream polymerization reactor at Carmel Olefins Ltd., in Haifa Bay. The 143-tray column is equipped with a heat pump, which compresses the vapor overheads, thus converting mechanical compression into thermal energy, which provides the reboiler duty. After expansion, the overheads are split between the top product and the columns reflux. A simplified flowsheet for the process, including the current control configuration, is shown in Figure 1. The output variables are P, the column pressure, y_D and x_B, the weight percentages of propane in the top product and propylene in the bottoms, respectively. The six potential manipulated variables are: F, F_{FCC}, the two feed flow rates, F_B, the bottoms flow rate, F_R, the reflux flow rate, C_D, the compressor duty, and F_C, the reboiler bypass flow rate. Both of the feed compositions and enthalpies, the cooling water supply temperature are treated as disturbances. Table 1 summarizes the flow rates and compositions of the two column feeds F and F_{FCC}, and also indicates the required product purities.

Table 1. Nominal Column Feeds and Product Specifications

		F	F_{FCC}	F_D	F_B
Flow Rate (% of total)		57	43	87	13
Compositions (wt %)	Propylene	93	78	98	11
	Propane	7	21	2	86
	Butylene	0	1	0	3

The current control configuration, indicated in **Figure 1**, includes direct flow control of R, control of top and bottom products by direct flow manipulation of the product streams D and B, respectively, temperature control of Cooler 2 output stream, T_R, by bypass flow, and pressure control at the column top by Cooler 1 (the trim condenser) output stream flow manipulation, F_C. The regulatory response for this configuration is very poor, with both product compositions exhibiting extreme oscillations in response to most of the process disturbances and upsets. A C&R analysis was commissioned to investigate the problem and suggest alternative control configurations to improve regulatory performance.

3 Short-cut Process Dynamic Model

A steady state model for the column is generated using HYSYS by Hyprotech Inc., and verified against plant data. The steady state simulation assumes constant pressures, which precludes the generation of short-cut dynamic model that accounts for the pressure dynamics. Therefore, the C&R analysis implies perfect pressure control, which is quite reasonable on inspection of plant transient data, where most of the time the pressure is almost constant. Moreover, the pressure dynamics are much quicker than the column dynamics and may be decoupled from the latter (Muhrer *et al.*, 1990). Thus, one manipulated variable must be reserved for pressure control, and following previous studies (Shinskey, 1984, Muhrer *et al.*, 1990), the appropriate variable is the cooling rate in the trim condenser, This is also the approach adopted in the plant, as indicated by the pressure controller, PC, in Figure 1. Thus, the problem is reduced to the regulation of the two remaining output variables, y_D and x_B.

An approximate dynamic model, accounting for the heat pump heat integration is developed using the approach described by Weitz and Lewin (1996). For this application, two *component parts* are required, modeling the "column" and the "heat pump": the former consists only of the column trays, while the latter models all of the remaining equipment items. Figure 2 shows the partitioning of the flowsheet into its component parts. In so doing, the process variables are divided into three vectors: $\underline{UD}$, containing all of the manipulated variable and disturbances, $\underline{CH}$, containing the internal variables transferring information between "column" and "heat pump", and $\underline{HC}$, fulfilling the same role between "heat pump" and "column".

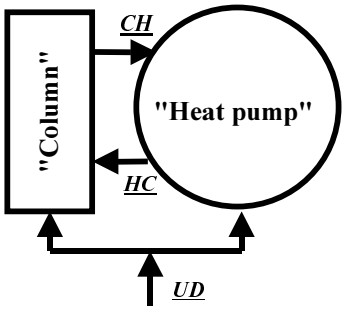

Figure 2. Partitioning the process into its component parts.

After careful study, the latter two vectors were defined as follows:

$\underline{CH} = [\, F_1, y_D, F_2, x_2, x_B \,]^T$, where F_1 and F_2 are the flow rates of streams 1 and 2 (see Figure 1), y_D and x_B, are the weight percentages of propane in the top product and propylene in the bottoms, respectively, and x_2 is the propane weight percentage of stream 2.

$\underline{HC} = [E_V, F_V, x_V^1, x_V^2, E_R, y_R,]^T$, where E_V , F_V , x_V^1 and x_V^2 are the enthalpy, flow rate, and propylene and propane weight percentages of the boil-up stream, and E_R and y_R are the enthalpy and propane weight percentage of the reflux stream.

The short-cut linear dynamic model for the trays is derived following Weitz and Lewin (1996). The column dynamics are approximated by a single dominant time constant, computed as suggested by Shinskey (1984), while the heat pump dynamics are approximated by a second-order lag with relatively small time constants. These approximations are justifiable considering the large reflux flow rates on the one hand, and the large number of trays in the column, on the other. The static gains of the component-part transfer function matrices are generated as follows:

1. Each of the component part inputs is varied in the expected operating range, while maintaining the remainder of the inputs at their nominal values. The effect of these variations on each of the component part output variables are recorded.
2. A cubic spline interpolation polynomial is generated to approximate the variation of each output to each input: $y_i = y_{i,s}(u_j)$.
3. The static gain coefficients are then computed by symbolic differentiation of the interpolation polynomials computed at the operating point:

$$K_{ij} \equiv \frac{\Delta y_i}{\Delta u_j} \approx y'_{i,s}\left(u_j\right) \tag{2}$$

This approach is an improvement on that suggested by Weitz and Lewin (1996) in that it avoids perturbation analysis, whose accuracy is step-size dependent. Furthermore, it allows the impact of non-linearities to be assessed directly. Since Taylor series expansion for each static gain element is:

$$\frac{\Delta y_i}{\Delta u_j} = y'_{i,s}(u_j) + \frac{1}{2} y''_{i,s}(u_j)\Delta u_j + \frac{1}{6} y'''_{i,s}(u_j)\Delta u_j^2 + \ldots \tag{3}$$

Clearly an estimate of the uncertainty in the gain element is the truncation error:

$$\Delta K_{ij} \approx \frac{1}{2} y''_{i,s}(u_j)\Delta u_j + \frac{1}{6} y'''_{i,s}(u_j)\Delta u_j^2 + \ldots \tag{4}$$

Since the process outputs y_D and x_B, are members of the vector $\underline{CH}$, the overall process model in Eq.(1) is generated by expressing $\underline{CH}$ in terms of $\underline{UD}$:

$$\begin{cases} \underline{CH} = \left[\underline{\underline{\mathbf{C}}}_{11} \;\vdots\; \underline{\underline{\mathbf{C}}}_{12}\right]\begin{pmatrix} HC \\ \underline{UD} \end{pmatrix} \\ \underline{HC} = \left[\underline{\underline{\mathbf{H}}}_{11} \;\vdots\; \underline{\underline{\mathbf{H}}}_{12}\right]\begin{pmatrix} \underline{CH} \\ \underline{UD} \end{pmatrix} \end{cases} \Rightarrow \underline{CH} = (\underline{\underline{\boldsymbol{I}}} - \underline{\underline{\mathbf{C}}}_{11}\underline{\underline{\mathbf{H}}}_{11})^{-1}(\underline{\underline{\mathbf{C}}}_{11}\underline{\underline{\mathbf{H}}}_{12} + \underline{\underline{\mathbf{C}}}_{12})\,\underline{UD} \tag{5}$$

The static gain coefficients of the matrices $\underline{\underline{\mathbf{C}}}_{11}$, $\underline{\underline{\mathbf{C}}}_{12}$, $\underline{\underline{\mathbf{H}}}_{11}$ and $\underline{\underline{\mathbf{H}}}_{12}$ are given in **Table 2**. The method used to estimate their dynamic components are discussed next.

Following Shinskey (1984), the column composition dynamics are approximated by a lumped parameter model, with a dominant time constant:

$$\tau = \frac{M_L}{F}, \tag{6}$$

where M_L, is the total trays liquid hold-up and F is the total column feed. Due to the large size of column, the vapor hold-up is significant (Muhrer *et al*., 1990) and is taken into consideration when estimating the effective column time constant:

$$\tau_C = \frac{M_L + M_V}{F} \tag{7}$$

where M_V is the total tray vapor hold-up, and τ_C is the effective column composition time constant. The liquid and vapor tray hydrodynamics are also approximated by lumped parameter model for each tray. The hydraulic time delays are calculated using the approach suggested by Shinskey (1984):

$$\theta = \frac{d(M_L)/dt}{d(L)/dt} = \frac{A\, d\, h_{ow}}{dL} \tag{8}$$

where L, is the liquid supply to the tray, h_{ow}, is the weir overflow, and A is the weir cross section. Using the Francis formula (h_{ow} = (L/(111 l_w))$^{2/3}$, where l_w is the weir length), the time delay associated with a single tray is:

$$\theta = \frac{2A}{333 l_w \sqrt{h_{ow}}} \tag{9}$$

Due to the small temperature differences along the column, a direct measure of product composition is required (e.g., by chromatography), modeled by 5 min time delays. The resulting transfer functions for each component part are given in the **Appendix**.

Table 2. Static Gains for the Component Parts.

(a) Column

Variable	F_1	y_D	F_2	x_2	x_B	
	CH					
E_V	3.1	0.039	–3.1	0.21	–0.22	HC
F_V	0.51	7.0×10^{-3}	0.49	0.035	–0.036	
x_V^1	90	6.3	–90	3.9	–3.9	
x_V^2	–93	–3.0	93	–6.2	6.5	
E_R	1.7	0.023	–1.7	0.12	–0.12	
y_R	49	1.6	–49	3.4	–3.5	
F	–0.012	-7.7×10^{-3}	1.0	–0.068	0.071	*UD*
F_{FCC}	0.32	4.8×10^{-4}	0.68	–0.034	0.035	
F_R	0.12	–0.012	0.88	–0.060	0.063	
E_{FCC}	0.063	8.1×10^{-4}	–0.063	4.3×10^{-3}	-4.5×10^{-3}	
z_{FCC}^1	1.8	0.026	-1.8	0.14	–0.15	
z_{FCC}^2	–1.7	–0.025	1.7	–0.14	0.14	
E_F	0.083	1.1×10^{-3}	–0.083	5.7×10^{-3}	-5.9×10^{-3}	
z_F	2.4	0.042	–2.4	0.18	–0.19	

(b) Heat Pump

Variable	E_V	F_V	x_V^1	x_V^2	E_R	y_R	
	HC						
F_B	0.11	–1.0	0.0	0.0	1.7×10^{-5}	0.0	*UD*
C_D	1.1	0.0	0.0	0.0	0.047	0.0	
T_{CW}	0.0	0.0	0.0	0.0	-4.0×10^{-6}	0.0	
F_C	–0.15	0.0	0.0	0.0	3.1×10^{-4}	0.0	
F_1	–0.38	0.0	0.0	0.0	0.68	0.0	*CH*
y_D	1.1	0.0	0.0	0.0	–28	1.0	
F_2	–0.11	1.0	0.0	0.0	2.8×10^{-3}	0.0	
x_2	–29	0.0	1.0	–0.77	5.2×10^{-5}	0.0	
x_B	32	0.0	–0.96	1.0	0.14	0.0	

The approach described in **Section 3** generates steady-state gains that individually exhibit up to 30% uncertainty. For example, consider **Figure 3**, which shows the variation of y_D with changes in E_R. In all, a total of six gain coefficient values in the component part matrices are observed to have significant uncertainty (over 5%). The study of the impact of these individual gain uncertainties on that of the overall transfer functions must account for the interdependencies between them, and is under investigation.

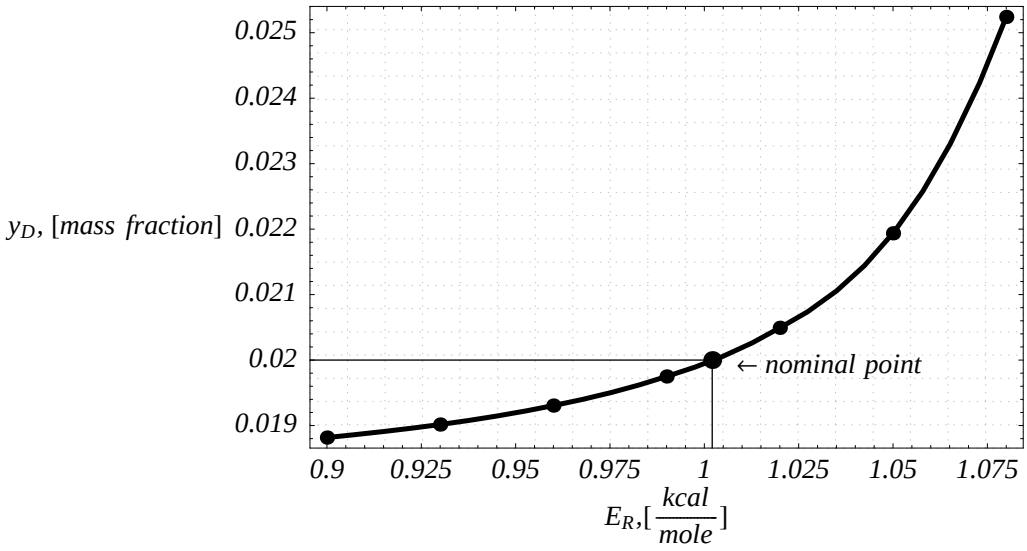

Figure 3. Example of gain uncertainty

4 Stability Analysis of the Operating Point

It is well known that the presence of positive feedback has a destabilizing effect on the process open-loop dynamics. For the linear system under investigation, its influence is assessed directly by computing the poles of the overall transfer matrix in Eq.(5). Since all of the component part matrices have stable poles, this requires only the poles of $(\boldsymbol{I} - \underline{\underline{\mathbf{C}}}_{11}\underline{\underline{\mathbf{H}}}_{11})^{-1}$ to be tested. Thus, for stability analysis, it is enough to investigate the existence of right-half-plane zeros of the expression: $| I - \underline{\underline{\mathbf{C}}}_{11}\underline{\underline{\mathbf{H}}}_{11}| = Z(s)$. Noting that all component part matrix elements are strictly proper, $Z(\infty)=1$. Consequently, if Z(0) is negative, this implies the existence of at least one right-half-place zero in Z(s), which in turn indicates that the overall system in open loop unstable. Finally, the number of clock-wise encirclements of the origin of the Nyquist plot indicates the number of right-half plane system poles. As shown in **Figure 4**, the nominal dynamics of the heat-integrated column indicate the presence of right half plane zeros. Furthermore, analysis shows that existence of at least one right-half-plane zero when considering all of the significant uncertainties on the individual gain elements. This result is in good agreement with that of Koggersbøl *et al.* (1996), who also studied heat integrated distillation column with a heat pump.

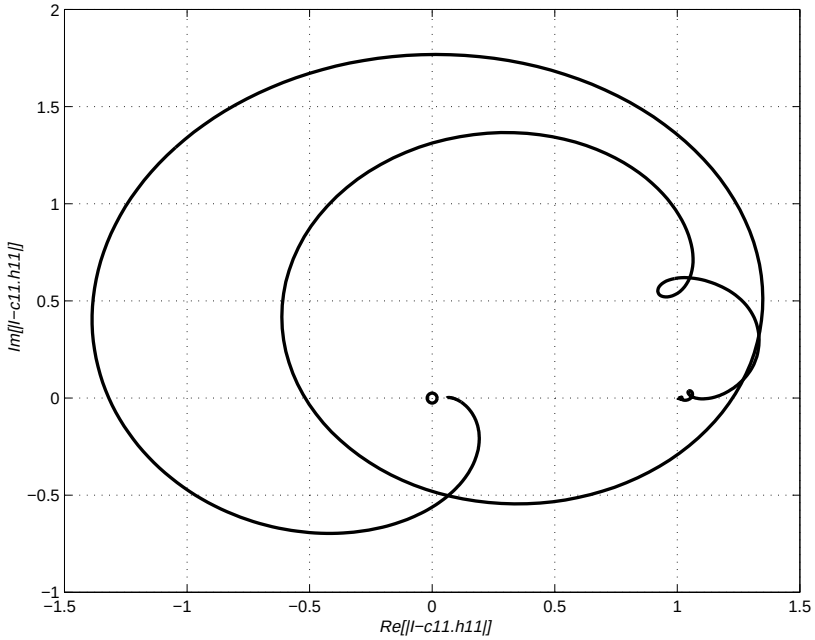

Figure 4. Nominal Nyquist plot

5 C&R Analysis Results

Having reserved the reboiler bypass flow, F_C, for overhead pressure control, this leaves five manipulated variables available for the control of the two remaining process outputs, which gives ten possible 2×2 decentralized control configurations $(5!/2!(5-2)!=10)$. **Table 3** defines these ten configurations according to the manipulated variable pair selected in each case.

Table 3. Ten possible 2×2 control configurations by manipulated variable pairs

A $\underline{\boldsymbol{u}} = [F, F_{FCC}]^{\mathrm{T}}$	B $\underline{\boldsymbol{u}} = [F, B]^{\mathrm{T}}$	C $\underline{\boldsymbol{u}} = [F, R]^{\mathrm{T}}$	D $\underline{\boldsymbol{u}} = [F, C_D]^{\mathrm{T}}$	E $\underline{\boldsymbol{u}} = [F_{FCC}, B]^{\mathrm{T}}$
F $\underline{\boldsymbol{u}} = [F_{FCC}, R]^{\mathrm{T}}$	G $\underline{\boldsymbol{u}} = [F_{FCC}, C_D]^{\mathrm{T}}$	H $\underline{\boldsymbol{u}} = [B, R]^{\mathrm{T}}$	I $\underline{\boldsymbol{u}} = [B, C_D]^{\mathrm{T}}$	J $\underline{\boldsymbol{u}} = [R, C_D]^{\mathrm{T}}$

The controllability of each of these configurations is tested based on two alternative implementations: (a) no temperature-control loop operational (i.e., the controller TC in **Figure 1** is in open loop), (b) temperature control is perfect. The recommended procedure for control configuration screening is as follows:

Step 1. Compute the worst case steady state DC for each configuration. Eliminate all configurations that cannot guarantee perfect steady-state disturbance rejection. Test the frequency-dependent DC for those configurations that are still under consideration.

Step 2. For all those configurations that are still under consideration, compute the static and frequency-dependent RGA. Eliminate all those that have poor bandwidth.

This procedure is now applied to select the most appropriate decentralized control configuration for the C_3 splitter.

Step 1: Disturbance Cost.

Following Lewin (1996), assuming perfect control ($\boldsymbol{y}(s) = 0$ in Eq.(1)), the control effort required to neutralize a multivariable disturbance:

$$\underline{\boldsymbol{u}}(s) = -\underline{\underline{\boldsymbol{P}}}^{-1}\underline{\underline{\boldsymbol{P}}}_d\underline{\boldsymbol{d}}(s) \tag{10}$$

The DC is the Euclidean norm of $\underline{\boldsymbol{u}}(s)$ computed as above. The steady state DCs shown in **Table 4** are computed for each manipulated variable separately, for the worst possible combinations of disturbances, and normalized to account for the effective operating range for each manipulated variable:

$$DC_i = \frac{|-\underline{\underline{\boldsymbol{P}}}^{-1}\underline{\underline{\boldsymbol{P}}}_d\bar{d}|_i}{U_i} \tag{11}$$

where $\bar{d}$ is the worst case disturbance vector, and U_i is the change that can be effected to the given manipulated variable without exceeding the operating limits of any given internal variable in the system. This is carried out systematically, by checking the effect of perturbations on each manipulated variable on all of the internal variables. For example, the nominal value of the reflux flow rate is 346 ton/h, but over-all gain between it and boil-up flow rate is 230 [boil-up ton/h / reflux ton/h]. The nominal value of the boil-up flow rate is 660 ton/h. Clearly, to maintain the boil-up within its physical limits, the reflux change must be limited to be less than $660/230 \approx 3$ ton/h. **Table 5** gives the nominal values of all of the disturbance variables, and the deviation levels assumed.

Table 4. Steady state DCs for all 2×2 control configurations

(a) No temperature control

A	B	C	D	E
[2.27,1.38]	[1.83,1.60]	[0.98,7.7]	[0.98,7.3]	[5.7,8.2]
F	G	H	I	J
[0.41,5.4]	[0.41,5.1]	[0.56,5.0]	[0.56,4.8]	[8800, 8400]

(b) Perfect temperature control

A	B	C	D	E
[0.23,0.69]	[0.18,0.79]	[0.55,4.0]	[0.55,3.9]	[0.87,1.3]
F	G	H	I	J
[0.48,1.2]	[0.48,1.2]	[0.67,1.1]	[0.67,1.1]	[670,660]

From **Table 4**, none of the configurations can guarantee offset-free disturbance rejection if temperature control is not implemented, since at least one of the control variables exceeds its constraints when challenged with the worst-case disturbance. However, if perfect temperature is assumed, two configurations are possible, namely A and B. The frequency-dependent DCs for these configurations are given in **Figure 5**, where at every frequency, the DC was evaluated using the Euclidean norm for the worst possible disturbance vector direction. Evidently, both configurations

will have poor disturbance-rejection bandwidths, indicating settling times of the order of 1500 min, even for the case of perfect control.

Table 5. Nominal disturbance variable values and assumed deviations.

Variable	Nominal	Deviation
T_{CW}	28 °C	±3°C
E_{FCC}	–3.78 kcal/mole	±0.01 kcal/mole
$z_{FCC}{}^{1}$	0.21	±0.01
$z_{FCC}{}^{2}$	0.78	±0.01
E_F	–0.88 kcal/mole	±0.01 kcal/mole
z_F	0.07	±0.01
F_C	22.32 ton/h	±5 ton/h

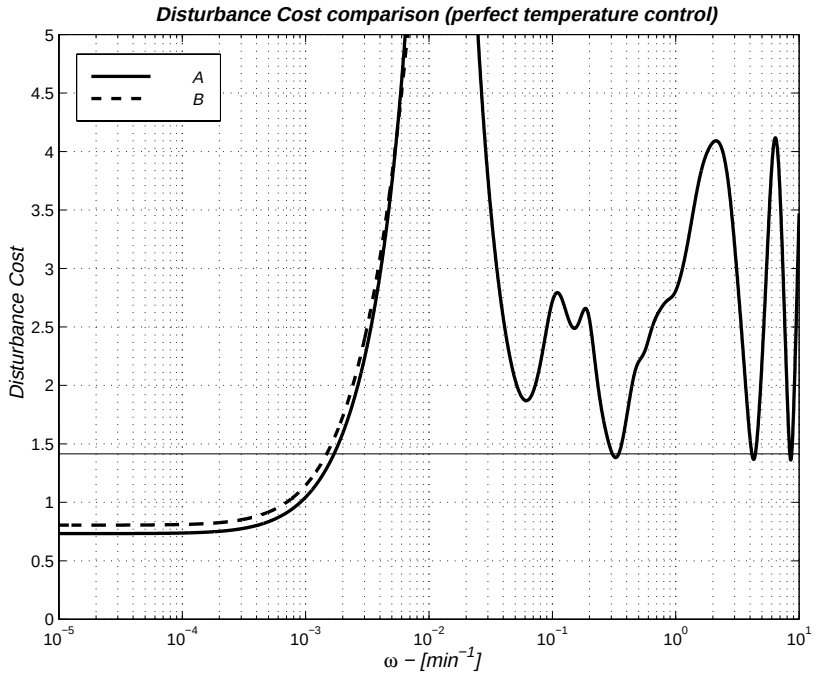

Figure 5. Frequency-dependent DCs for configurations guaranteeing static disturbance rejection

Step 2: Relative Gain Array

Bristol (1966) introduced the RGA as a controllability measure, which relies on perfect control assumptions. The RGA, $\underline{\Lambda}$, is a square matrix comprising of coefficients, λ_{ij}, each of which is the ratio:

$$\lambda_{ij} = \frac{\text{process gain between input } j \text{ and output } i \text{ when all other control loops are open}}{\text{process gain between input } j \text{ and output } i \text{ when all other control loops are perfectly controlled}}$$

Clearly, it is advantageous to select decentralized control pairings *i-j*, such that λ_{ij} is close to unity in the frequency range where performance is sought. Pairings with negative λ_{ij} coefficients should be avoided, since they imply an effective polarity change as seen by the controller acting on that pairing

when the status of other loops in the process are changed (e.g., from automatic to manual).. Mathematically, the RGA is computed as:

$$\underline{\underline{\Lambda}} = \underline{\underline{P}}(s) \otimes [\underline{\underline{P}}(s)^{-1}]^{T}, \tag{11}$$

where ⊗ indicates element by element product The steady state RGAs for configurations A and B for perfect temperature control are given in **Table 6**.

Table 6. Steady state RGA for perfect temperature control.

A	B
$\Lambda_{11} = 1.17$	$\Lambda_{11} = 1.15$

The results in **Table 6** indicate that both decentralized configurations A and B are almost perfectly decoupled at steady state, and that if implemented, must be paired diagonally. In contrast, **Figure 6** shows frequency-dependent RGA for these configurations, which show that significant bandwidth limitation can be expected with both schemes.

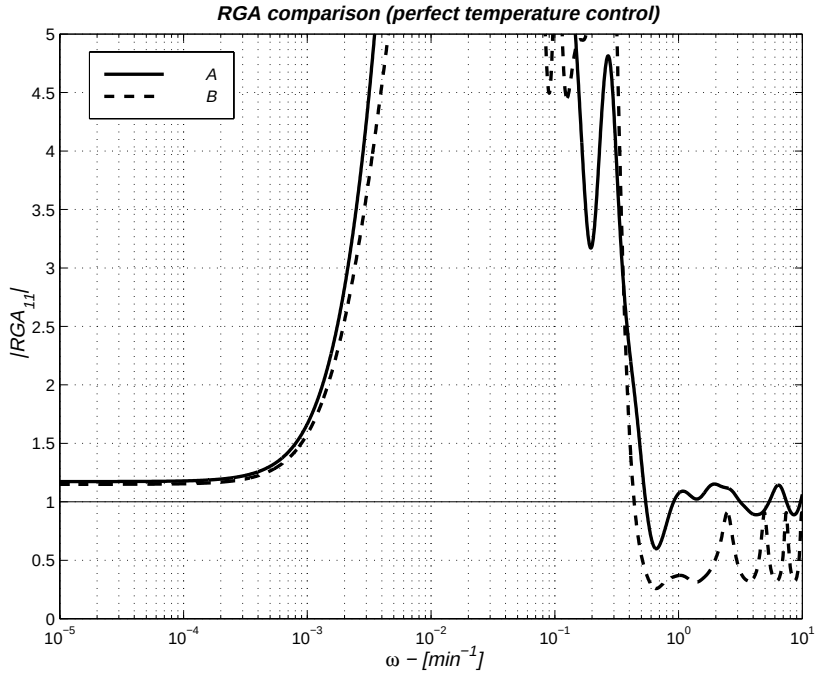

Figure 6. Frequency-dependent RGAs for configurations guaranteeing static disturbance rejection

6 Conclusions and Recommendations

The results of the C&R analysis for the C_3 splitter are:

a) The current operating point is open loop unstable. The most important task encumbering the control system is to stabilize this. It is noted that the current control configuration does not achieve this task, requiring significant manual operator intervention.

b) The C&R analysis has eliminated all decentralized control configurations other than A and B, and has indicated that tight control on the reflux return temperature is mandatory. The focus on con-

figuration A is interesting in that this is the current policy adopted by the plant operators, who commonly manipulate both of the feed flow rates manually, in an attempt to stabilize the process.

c) Because of the bandwidth limitations imposed by dynamic interactions, and the need for significant feedback to stabilize the open-loop unstable process, it is clearly impossible to adequately control this system using decentralized control. It is recommended that a non-square MPC control system be designed, using all of the available manipulated variables (F, F_{FCC}, F_B, F_R, and C_D) to meet the process specifications (y_D and x_B). The MPC controller should also include feedforward elements to enhance the rather poor disturbance-rejection performance that would otherwise be achievable using only feedback.

d) The local gain uncertainties can change the sign of the overall gains. The impact of the local gain uncertainties on the overall process gains requires further investigation.

Acknowledgements

This research was carried out with the support of Carmel Olefins Ltd., Haifa. The authors wish to acknowledge the encouragement of the Plant Manager, Zvi A. Jaeger, and the valuable inputs of the Ethylene Plant Manager, David Dori and the plant engineers, Dorit Kashy and Gil Pinchas.

7 References

Bristol, E. H. (1966). "On a New Measure of Interactions for Multivariable Process Control", *IEEE Trans. Automatic. Control*, **AC -11**,133-134

Koggersbøl, A., B. R. Andersen, J. S. Nielsen, and S. Bay Jørgensen (1996). "Control Configurations for an Energy Integrated Distillation Column", *Comp. and Chem. Engnrg*, **20**(S), S853-S858

Lewin, D. R. (1996). "A Simple Tool for Disturbance Resiliency Diagnosis and Feedforward Control Design", *Comp. and Chem. Engnrg.* **20,**13-25

Lewin, D. R. and D. Bogle (1996). "Controllability Analysis of an Industrial Polymerization Reactor", *Comput. Chem. Eng.*, **20**(S), S871-S876

Lewin, D. R., J.-P. Gong, and R. Gani (1996). "Optimal Design and Controllability Assessment for a Plant-wide Benchmark", *Proc. of the 13th IFAC World Congress*, **M**, 79-84

Lewin, D. R (1999). "Integration of Design and Control" *Proc. of the 7th IEEE Mediterranean Conference on Control and Automation* (MED'99), Haifa

Muhrer, C. A., M. A. Collura and W. L. Luyben (1990). "Control of Vapor Recompression Distillation Column", *Ind. Eng. Chem. Res.*, **29,** 59-71

Naot, I. and D. R. Lewin (1995). "Analysis of Process Dynamics in Recycle Systems using Steady State Flowsheeting Tools", *Proc. of the 4th IFAC Symp. on Dynamics and Control of Chemical Reactors, Distillation Columns and Batch Processes* (*DYCORD+ '95*), Helsingør

Seider W. D., J. D. Seader and D. R. Lewin (1999). *Process Design Principles: Synthesis, Analysis and Evaluation*, John Wiley and Sons

Shinskey, F. G. (1984). "Distillation Control For Productivity and Energy Conservation", *McGraw-Hill*, 56, 82-89

Solovyev, B. M., R. Miller, G. Emoto and D. R. Lewin (1998). "Ethylene Quench Column Optimal Operation and Controllability Analysis", *Proc. of the 5th IFAC Symposium of Dynamics and Control of Processing Systems* (*DYCOPS'5*)

Weitz, O. and Lewin, D. R. (1994). "Dynamic Controllability and Resiliency Diagnosis using Steady State Process Flowsheet Data", *Comput. Chem. Eng.*, **20**(4), 325-335.

Weitz, O. (1994). *Integrating Controllability Measures into Process Design*, M.Sc. Thesis, Technion.

Appendix: Linear Component Part Dynamics

$$\mathbf{C_{11}} = \begin{pmatrix} \frac{3.05873}{(\frac{7s}{143}+1)^{143}} & \frac{0.50692}{(\frac{7s}{143}+1)^{143}} & \frac{89.594}{(\frac{7s}{143}+1)^{143}} & -\frac{92.6225}{(\frac{7s}{143}+1)^{143}} & \frac{1.73103}{\frac{7s}{143}+1} & \frac{49.3232}{\frac{7s}{143}+1} \\ \frac{0.0391225\,e^{-5s}}{45s+1} & \frac{0.00697548\,e^{-5s}}{45s+1} & \frac{6.32848\,e^{-5s}}{45s+1} & -\frac{2.9558\,e^{-5s}}{45s+1} & \frac{0.0226649\,e^{-5s}}{45s+1} & \frac{1.57211\,e^{-5s}}{45s+1} \\ -\frac{3.05872}{\frac{45s}{143}+1} & \frac{0.49308}{\frac{45s}{143}+1} & -\frac{89.594}{\frac{45s}{143}+1} & \frac{92.6225}{\frac{45s}{143}+1} & -\frac{1.73103\,e^{-7s}}{(\frac{45s}{143}+1)^{143}} & -\frac{49.3232\,e^{-7s}}{(\frac{45s}{143}+1)^{143}} \\ \frac{0.209956\,e^{-5s}}{45s+1} & \frac{0.0345086\,e^{-5s}}{45s+1} & \frac{3.86195\,e^{-5s}}{45s+1} & -\frac{6.2165\,e^{-5s}}{45s+1} & \frac{0.118529\,e^{-12s}}{45s+1} & \frac{3.37981\,e^{-12s}}{45s+1} \\ -\frac{0.219059\,e^{-5s}}{45s+1} & -\frac{0.0360173\,e^{-5s}}{45s+1} & -\frac{3.90056\,e^{-5s}}{45s+1} & \frac{6.52895\,e^{-5s}}{45s+1} & -\frac{0.123681\,e^{-12s}}{45s+1} & -\frac{3.5266\,e^{-12s}}{45s+1} \end{pmatrix}$$

$$\mathbf{C_{12}} = \begin{pmatrix} -\frac{0.0116242}{(\frac{7s}{143}+1)^{91}} & \frac{0.324935}{(\frac{7s}{143}+1)^{61}} & \frac{0.122992}{\frac{7s}{143}+1} & \frac{0.0627714}{(\frac{7s}{143}+1)^{61}} & \frac{1.80387}{(\frac{7s}{143}+1)^{61}} & -\frac{1.73991}{(\frac{7s}{143}+1)^{61}} & \frac{0.0828308}{(\frac{7s}{143}+1)^{91}} & \frac{2.35685}{(\frac{7s}{143}+1)^{91}} & 0 & 0 & 0 & 0 \\ -\frac{0.00766661\,e^{-5s}}{45s+1} & \frac{0.000480178\,e^{-5s}}{45s+1} & -\frac{0.0116464\,e^{-5s}}{45s+1} & \frac{0.000806484\,e^{-5s}}{45s+1} & \frac{0.02638\,e^{-5s}}{45s+1} & -\frac{0.0251144\,e^{-5s}}{45s+1} & \frac{0.00107736\,e^{-5s}}{45s+1} & \frac{0.0421815\,e^{-5s}}{45s+1} & 0 & 0 & 0 & 0 \\ \frac{1.01162\,e^{-28s/11}}{(\frac{45s}{143}+1)^{52}} & \frac{0.675065\,e^{-574s/143}}{(\frac{45s}{143}+1)^{82}} & \frac{0.877008\,e^{-7s}}{(\frac{45s}{143}+1)^{143}} & -\frac{0.0627695\,e^{-574s/143}}{(\frac{45s}{143}+1)^{82}} & -\frac{1.80387\,e^{-574s/143}}{(\frac{45s}{143}+1)^{82}} & \frac{1.73991\,e^{-574s/143}}{(\frac{45s}{143}+1)^{82}} & -\frac{0.0828297\,e^{-28s/11}}{(\frac{45s}{143}+1)^{52}} & -\frac{2.35685\,e^{-28s/11}}{(\frac{45s}{143}+1)^{52}} & 0 & 0 & 0 & 0 \\ -\frac{0.0679356\,e^{-83s/11}}{45s+1} & -\frac{0.0343358\,e^{-1289s/143}}{45s+1} & -\frac{0.0599523\,e^{-12s}}{45s+1} & \frac{0.00430627\,e^{-1289s/143}}{45s+1} & \frac{0.141582\,e^{-1289s/143}}{45s+1} & -\frac{0.136564\,e^{-1289s/143}}{45s+1} & \frac{0.00567551\,e^{-83s/11}}{45s+1} & \frac{0.180574\,e^{-83s/11}}{45s+1} & 0 & 0 & 0 & 0 \\ \frac{0.0709463\,e^{-83s/11}}{45s+1} & \frac{0.035437\,e^{-1289s/143}}{45s+1} & \frac{0.0625623\,e^{-12s}}{45s+1} & -\frac{0.00449354\,e^{-1289s/143}}{45s+1} & -\frac{0.146701\,e^{-1289s/143}}{45s+1} & \frac{0.142637\,e^{-1289s/143}}{45s+1} & -\frac{0.00592217\,e^{-83s/11}}{45s+1} & -\frac{0.187588\,e^{-83s/11}}{45s+1} & 0 & 0 & 0 & 0 \end{pmatrix}$$

$$\mathbf{H_{11}} = \begin{pmatrix} -\frac{0.378834}{(5s+1)^2} & \frac{1.10827}{(5s+1)^2} & -\frac{0.113702}{(5s+1)^2} & -\frac{28.5968}{(5s+1)^2} & \frac{31.9479}{(5s+1)^2} \\ \frac{0.}{(5s+1)^2} & \frac{0.}{(5s+1)^2} & \frac{1.}{(5s+1)^2} & \frac{0.}{(5s+1)^2} & \frac{0.}{(5s+1)^2} \\ \frac{0.}{(5s+1)^2} & \frac{0.}{(5s+1)^2} & \frac{0.}{(5s+1)^2} & \frac{1.}{(5s+1)^2} & -\frac{0.963165}{(5s+1)^2} \\ \frac{0.}{(5s+1)^2} & \frac{0.}{(5s+1)^2} & \frac{0.}{(5s+1)^2} & -\frac{0.770402}{(5s+1)^2} & \frac{1.}{(5s+1)^2} \\ \frac{0.682755}{(5s+1)^2} & -\frac{28.408}{(5s+1)^2} & \frac{0.00281496}{(5s+1)^2} & \frac{0.0000520156}{(5s+1)^2} & \frac{0.138219}{(5s+1)^2} \\ \frac{0.}{(5s+1)^2} & \frac{1.}{(5s+1)^2} & \frac{0.}{(5s+1)^2} & \frac{0.}{(5s+1)^2} & \frac{0.}{(5s+1)^2} \end{pmatrix}$$

$$\mathbf{H_{12}} = \begin{pmatrix} 0 & 0 & 0 & 0 & 0 & 0 & 0 & 0 & \frac{0.113337}{(5s+1)^2} & \frac{1.12173}{(5s+1)^2} & \frac{0.}{(5s+1)^2} & -\frac{0.149768}{(5s+1)^2} \\ 0 & 0 & 0 & 0 & 0 & 0 & 0 & 0 & -\frac{1.}{(5s+1)^2} & \frac{0.}{(5s+1)^2} & \frac{0.}{(5s+1)^2} & \frac{0.}{(5s+1)^2} \\ 0 & 0 & 0 & 0 & 0 & 0 & 0 & 0 & \frac{0.}{(5s+1)^2} & \frac{0.}{(5s+1)^2} & \frac{0.}{(5s+1)^2} & \frac{0.}{(5s+1)^2} \\ 0 & 0 & 0 & 0 & 0 & 0 & 0 & 0 & \frac{0.}{(5s+1)^2} & \frac{0.}{(5s+1)^2} & \frac{0.}{(5s+1)^2} & \frac{0.}{(5s+1)^2} \\ 0 & 0 & 0 & 0 & 0 & 0 & 0 & 0 & \frac{0.0000166596}{(5s+1)^2} & \frac{0.0472259}{(5s+1)^2} & -\frac{3.96037\times10^{-6}}{(5s+1)^2} & \frac{0.000305634}{(5s+1)^2} \\ 0 & 0 & 0 & 0 & 0 & 0 & 0 & 0 & \frac{0.}{(5s+1)^2} & \frac{0.}{(5s+1)^2} & \frac{0.}{(5s+1)^2} & \frac{0.}{(5s+1)^2} \end{pmatrix}$$